

Window and inpainting: dealing with data gaps for TianQin

Lu Wang,¹ Hong-Yu Chen,¹ Xiangyu Lyu,¹ En-Kun Li,^{1,*} and Yi-Ming Hu^{1,†}

¹*MOE Key Laboratory of TianQin Mission, TianQin Research Center for Gravitational Physics & School of Physics and Astronomy, Frontiers Science Center for TianQin, gravitational wave Research Center of CNSA, Sun Yat-sen University (Zhuhai Campus), Zhuhai 519082, China*

Space-borne gravitational wave detectors like TianQin might encounter data gaps due to factors like micro-meteoroid collisions or hardware failures. Such glitches will cause discontinuity in the data and have been observed in the LISA Pathfinder. The existence of such data gaps presents challenges to the data analysis for TianQin, especially for massive black hole binary mergers, since its signal-to-noise ratio (SNR) accumulates in a non-linear way, a gap near the merger could lead to significant loss of SNR. It could introduce bias in the estimate of noise properties, and furthermore the results of the parameter estimation. In this work, using simulated TianQin data with injected a massive black hole binary merger, we study the window function method, and for the first time, the inpainting method to cope with the data gap, and an iterative estimate scheme is designed to properly estimate the noise spectrum. We find that both methods can properly estimate noise and signal parameters. The easy-to-implement window function method can already perform well, except that it will sacrifice some SNR due to the adoption of the window. The inpainting method is slower, but it can minimize the impact of the data gap.

I. INTRODUCTION

Space-borne gravitational wave (GW) detectors like TianQin [1] and LISA [2] have the potential to greatly expand and even revolutionize our observational capabilities to our Universe, enabling the detection of GW signals in the millihertz (mHz) frequency band. Detecting and analyzing these signals will illuminate the fundamental properties of the Universe and provide distinctive insights into the nature of spacetime.

TianQin is a space-borne GW mission comprising three satellites. The mission is expected to be launched in the 2030s. These satellites will form an equilateral triangle constellation in a geocentric orbit, with a radius of about 100,000 km and an arm-length of roughly 170,000 km. The constellation's plane will be oriented towards the reference source RX J0806.3+1527 binary system [1]. The mission will operate on a “3 months on + 3 months off” scheme [1]. Its goal is to detect GW sources within the frequency band of 0.1 mHz to 1 Hz, including the coalescence of massive black hole binaries (MBHBs) [3–6], the inspiral of double white dwarfs [7, 8], stellar-mass binary black hole inspiral [9, 10], extreme mass ratio inspirals (EMRIs) [11], and the stochastic GW background [12, 13].

Among these sources, MBHB is one of the primary objectives for space-borne detectors. Observational evidence indicates the ubiquitous presence of massive black hole (MBH) in the nuclei of galaxies, and it is hypothesized that triggered by the galaxy collisions, these central MBHs will ultimately be drawn together and collide [14, 15]. However, our understanding of the formation and growth of the MBHBs are constantly challenged and

refreshed by the observations [e.g. 16]. Detecting gravitational waves from MBHBs has the potential to pinpoint the formation mechanism [3, 17], depict properties of black holes in details [18, 19], and decipher the growth history of the Universe [20].

The aforementioned scientific promises are often predicted upon idealized assumptions on the GW detector's data, like the Gaussianity and stationarity. However, GW detectors encounter challenges due to periods of missing information during observations, commonly referred to as “data gaps” and thus the data do not meet the prerequisites of Gaussianity and stationarity any longer [21]. The data gaps could be caused by scheduled or scheduled factors. Scheduled gaps are typically due to device maintenance work. For instance, laser interferometer gravitational-wave observatory (LIGO) may suspend observations temporarily for instrument upgrades and repairs, resulting in scheduled gaps [22]. Similarly, LISA may experience scheduled gaps during high-gain antenna repointing and laser frequency relocking processes [23, 24], as well as periodic test mass (TM) discharge processes to get rid of charges accumulated through the interaction with the cosmic rays [25–28]. Unlike the LISA mission, TianQin operates in a geocentric orbit, with its antenna consistently pointing toward the Earth, eliminating the need for periodic antenna adjustment [29]. Furthermore, a continuous discharge strategy could be adopted to address the issue of charge accumulation on the TMs [30]. Therefore, in the ideal scenario, TianQin could totally avoid scheduled data gaps during observations. Unscheduled gaps may result from equipment failure or external disturbances, such as seismic interference [31] and micrometeorite collisions [32–35]. In addition, non-stationarity of the data could appear in the form of glitches, which have been widely observed in GW detectors' data [36–40]. A straightforward way to deal with glitches is to gate the data, effectively introducing gaps in the data.

* lienk@sysu.edu.cn

† huyiming@sysu.edu.cn

Up till now, most of the GW events reported in the ground-based detectors are much shorter than a typical gap. It is reasonable then to assume that a signal is either totally missed in the gap or fully present in the continuous data stream. However, for space-borne GW missions, most of the signals could persist in the data for extended periods, ranging from several hours to even years. This extended duration significantly increases the probability of data gaps intersecting with these signals, thereby posing a greater challenge in terms of data continuity and signal analysis [21, 41]. For example, the data gap could lead to spectral leakage in the frequency domain, contaminating other signals [42]. Secondly, the estimation of the noise’s power spectral density (PSD) might need constant updates, due to the changing antenna pattern relative to the anisotropic Galactic foreground, which renders the time-dependant PSD. If the gap frequently happens, many of the data chunks would not be long enough to cover the lower end of the GW spectrum, making the task of PSD estimation much harder. The issue becomes more challenging for MBHBs, which accumulates signal-to-noise ratio (SNR) in a highly non-linear fashion as the merger time approaches [4]. A data gap occurring during the merger would result in a significant SNR loss, potentially leading to significant bias in parameter estimation [21].

There have been several pioneering works that aim to alleviate the effect of data gaps for space-borne GW detectors. This method is simple to operate, however, the suppression of spectral leakage is not complete and may result in the loss of data [43] and disruption of the Gaussian stationary characteristics of the noise. The window function method was the earliest to be adopted and simplest to implement [21, 23, 42], the major drawback is it will result in the loss of valid data points. Earlier studies like Baghi et al. [23], Carré and Porter [42] claim that using the window function method for gap data processing introduces a bias that can be as large as 9%. However, such a claim was not universally accepted, other studies like Dey et al. [21] indicate that the window function method can be bias-free. The Bayesian data augmentation (DA) method [41, 44] can update the guess of the missing data, which allows the estimate of the noise PSD and GW signals simultaneously. A third method is based on the sparsity framework [45], which allows for the estimation of both the signal and noise, followed by gap filling with the estimated data. Both the DA method and sparsity framework method sample the signal and the missing data, simultaneously. By doing so one can naturally account for the impact of the missing data through marginalization, with the cost of extra computational burden.

While these methods provide valuable solutions for managing gapped data in space-borne GW detectors, they come with challenges. Particularly, a trade-off exists between computational complexity and accuracy. Less computationally complex methods often struggle to ensure accurate likelihood calculation.

In recent years, the gating-and-inpainting technique has been applied to handle missing data issues for ground-based GW detectors, either for the treatment of noise transients [43, 46–48], or for delicate analysis of the ringdown signal [49–51]. Typically, it involves a “gating” process to eliminate unwanted data segments [52], followed by the “inpainting” stage for data interpolation. Mathematically, the inpainting technique that interpolates data and fills the gap is equivalent to masking the covariance matrix in likelihood calculation, so that the interpolated data does not bias the likelihood of the whole data. In principle, this method retains all information within the data and introduces minimal bias in the parameter estimation. The method naturally retains the continuity of the data, and it has additional advantage of retaining all existing useful data.

In this work, we aim to investigate whether the easy-to-implement window function methods can be bias-free. We also implement, for the first time, the gating-and-inpainting method to deal with the gap in space-borne GW detector data. Since the gap *per se* already act as a gating process, hereafter we refer to the method as the “inpainting” method.

The paper is organized as follows. In Sec. II, we introduce the statistical background of the study. theory of parameter estimation and perform a theoretical analysis of the impact of data gaps. In Sec. III, we detail the method, including the data generation, and the iterative algorithm estimating the noise PSD. Additionally, we present both the window function and the inpainting technique to solve the data gap problem. In Sec. IV, we present the result for a case study with a MBHB merger. Our conclusion and discussion are made in Sec. V.

II. STATISTICS BACKGROUND

A. Bayesian inference

The complete data \mathbf{d} recorded by a GW detector is sampled at regular intervals of Δt throughout data collection time T . And it can be represented as $\mathbf{d} = \{d_1, d_2, \dots, d_N\}$, which satisfy $T = (N - 1)\Delta t$. GW data consists of both signal and noise,

$$\mathbf{d}(t) = \mathbf{h}(t, \theta) + \mathbf{n}(t), \quad (1)$$

where $\mathbf{h}(t, \theta)$ represents the signal that depends on a set of parameters θ , $\mathbf{n}(t)$ is noise.

Under the frame of the Bayesian inference, the posterior probability $p(\theta|\mathbf{d})$ can be expressed as:

$$p(\theta|\mathbf{d}) = \frac{p(\mathbf{d}|\theta)p(\theta)}{p(\mathbf{d})} \quad (2)$$

where $p(\mathbf{d}|\theta)$ is the likelihood, $p(\theta)$ is the prior of the parameter θ , and $p(\mathbf{d})$ is the normalizing evidence.

For a Gaussian noise characterized by a $N \times N$ covariance matrix Σ , the time domain likelihood in logarithm

form can be written as:

$$\log p(\mathbf{d}|\theta) = -\frac{1}{2} [N \log 2\pi + \log |\boldsymbol{\Sigma}| + (\mathbf{d} - \mathbf{h}(\theta))^T \boldsymbol{\Sigma}^{-1} (\mathbf{d} - \mathbf{h}(\theta))]. \quad (3)$$

Typically, the computational complexity of inverting an $N \times N$ matrix is proportional to $O(N^3)$. This results in a large computational demand in computation time for large N . If the noise possesses not only Gaussian characteristics but also stationary characteristics, the covariance matrix in the time domain exhibits a Toeplitz structure, in other words, the elements along the diagonal direction are identical. Additionally, if we adopt the Whittle approximation that further treats the covariance matrix as circulant, which means that each row of the matrix is a right cyclic shift of the row above it [53], we can approximately obtain the diagonalization: $\boldsymbol{\Sigma} \approx W^\dagger \mathbf{\Lambda} W$, where W is the discrete Fourier matrix defined as $W_{jk} = N^{-1} \exp\left(-\frac{2\pi i j k}{N}\right)$, and W^\dagger is the Hermitian conjugate of W . $\mathbf{\Lambda}$ possesses the nice property of being a diagonal matrix, with its eigenvalues corresponding to the noise PSD S_n of the frequency domain, while the one-sided PSD $S_n(f)$ can be defined as

$$E[\tilde{\mathbf{n}}(f_i) \tilde{\mathbf{n}}^*(f_j)] = \frac{1}{2} T S_n(f_i) \delta_{ij}. \quad (4)$$

The inner product is defined by

$$(h_1|h_2) = 4 \sum_{i=1}^N \frac{h_1^*(f_i) h_2(f_i)}{S_n(f_i)} \quad (5)$$

Thus the log-likelihood can then be simplified as,

$$\log p(\mathbf{d}|\theta) \approx -\frac{1}{2} \left[N \log 2\pi + \log |\mathbf{\Lambda}| + (\mathbf{d} - \mathbf{h}_\theta | \mathbf{d} - \mathbf{h}_\theta) \right], \quad (6)$$

By employing the frequency domain likelihood and utilizing the fast Fourier transform algorithm, the computational complexity of the covariance matrix can be significantly reduced from $O(N^3)$ to $O(N \log N)$ [54].

B. Theoretical analysis of data gaps impact

In practice, the impact of data gaps on data processing is mainly reflected in two aspects. On the one hand, data gaps can lead to spectral leakage, as discussed in for example [21, 42, 45, 55]. On the other hand, due to the data gaps, the noise is no longer Gaussian and stationary, and the frequency approximation likelihood Eq. (6) is not applicable, thus necessitating the use of the time-domain likelihood function Eq. (3). When the data points are missing within the time range $t \in [t_{\text{gap}}^i, t_{\text{gap}}^f]$, the affected data is presented as:

$\mathbf{d}_{\text{gap}} = [d_1, \dots, d_{t_{\text{gap}}^i}, 0, \dots, 0, d_{t_{\text{gap}}^f}, \dots, d_N]$. This presence of zeros disrupts the Toeplitz structure of the covariance matrix $\boldsymbol{\Sigma}_{\text{gap}}$. Consequently, the likelihood expression in the frequency domain Eq. (6) is no longer valid.

III. METHOD

A. Data generation

In this manuscript, the IMRPhenomD waveform [56, 57] is used to generate the injected MBHB signals. The GW signal of a MBHB merger can be described by the following parameters: the luminosity distance D_L , the redshifted chirp mass M_c , the symmetric mass ratio η , the merger time t_c , the inclination angle ι , the polarization angle ψ , the ecliptic longitude λ , the ecliptic latitude β , and the coalescence phase ϕ_c . The response channels of detectors we adopted are time-delay interferometry (TDI) channels: A, E, and T [10, 58], which could be constructed by three Michelson-like variables, the X, Y, Z channel:

$$A = \frac{Z - X}{\sqrt{2}}, \quad E = \frac{X - 2Y + Z}{\sqrt{6}}, \quad T = \frac{X + Y + Z}{\sqrt{3}}. \quad (7)$$

The Michelson X channel [59] is composed of:

$$\begin{aligned} \mathbf{X}(t) = & [\Phi_{12}(t - 3L/c) + \Phi_{21}(t - 2L/c) + \Phi_{13}(t - L/c) \\ & + \Phi_{31}(t)] - [\Phi_{13}(t - 3L/c) + \Phi_{31}(t - 2L/c) \\ & + \Phi_{12}(t - L/c) + \Phi_{21}(t)], \end{aligned} \quad (8)$$

here Φ_{ij} represents the recorded laser phase from satellite i to satellite j , and L is the arm length of TianQin. The other Michelson observables Y, Z can be obtained through cyclic permutation.

The noise model adopts TDI channel (A) expressed in relative frequency [60]:

$$\begin{aligned} S_A(f) = & 8 \sin^2 u [4(1 + \cos u + \cos^2 u) \cdot S_{\text{acc}} \\ & + S_{\text{oms}}(\cos u + 2)], \\ \sqrt{S_{\text{oms}}} = & \sqrt{S_p} \frac{2\pi f}{c}, \\ \sqrt{S_{\text{acc}}} = & \frac{\sqrt{S_a}}{2\pi f c} \sqrt{1 + \left(\frac{0.1\text{mHz}}{f}\right)}. \end{aligned} \quad (9)$$

where $u = 2\pi f L/c$, the acceleration noise $S_a = 1 \times 10^{-30} \text{ m}^2/\text{s}^4/\text{Hz}$ and position noise $S_p = 1 \times 10^{-24} \text{ m}^2/\text{Hz}$ for TianQin.

To simulate the unscheduled gaps, previous studies focused on a 10-minute gap duration [21, 42, 45, 55]. In alignment with these studies, we have also chosen 10-minute gaps. Gapped data can be simulated by the product of the rectangular window function and the time-domain complete data

$$\mathbf{d}_{\text{gap}} = \mathbf{d} \cdot w(t), \quad (10)$$

where $w(t)$ is the rectangular window function:

$$w(t) = \begin{cases} 0, & t_{\text{gap}}^i < t < t_{\text{gap}}^f, \\ 1, & t < t_{\text{gap}}^i, t > t_{\text{gap}}^f, \end{cases} \quad (11)$$

here t_{gap}^i and t_{gap}^f represent the beginning and end of the gap respectively.

B. Iterative PSD Estimation

To obtain the unbiased estimation of the physical parameters of the sources, especially when the verdict of the gravity theory is at stake, accurate estimation of the noise PSD becomes a crucial task. Even though experimentalists will provide detailed modeling of the PSD, the actual onboard performance of the instruments can hardly be modeled reliably. Therefore, it is essential to estimate it from the actual data. Currently, noise PSD estimation can be categorized into two methods: off-source and on-source [13, 61–65].

The “off-source” data often employs the Welch method [66] to estimate the PSD from data around, but without, the source. This method averages the periodograms of several data segments, each of the same length as the signal while excluding the signal itself [67]. Under the assumption that the off-source data contains no GW signals, and the property of the PSD remains stable within a short enough time, this method provides a reliable estimate for the PSD. However, for space-borne GW detectors, the presence of overlapping long-lasting GW signals in the data makes the previous assumptions invalid, therefore one can not simply adopt the method.

The “on-source” data can be implemented in two ways: the first is the sequential estimation, where noise parameters are iteratively estimated from the data until a stable point estimation of the noise PSD is achieved. Subsequently, the posterior probability distribution of the signal parameters is explored using the point estimation of noise PSD, as has been implemented in BayesWave [23, 62–64] and FastSpec [68]. The other approach is simultaneous estimation, which explores the posterior probability distributions of both the signal and noise parameters simultaneously. Comparing the two methods, sequential estimation can provide conditional probabilities for source parameters, while simultaneous estimation provides marginal probabilities. Studies performed on ground-based detectors indicate that the above two have little difference, the peak position and the width of the posterior probabilities of the two methods differ by only a few percent [69–71].

Out of simplicity, in this study, we adopt the sequential estimation method to achieve a more rapid PSD estimation.

The algorithm splits into four steps, see Fig. 1:

Step 1 Data generation: Randomly generate noise according to an inject PSD, and inject MBHB merger signal, the combination is the simulated data. At this

stage, an initial guess of the PSD is also needed, but it is not necessarily similar to the inject PSD.

Step 2 Update signal: Using an optimizer to search for the best-matched signal template under the current knowledge of the PSD.

Step 3 Update PSD: Update the estimate of the noise PSD by analyzing the template-removed residual, under the current knowledge of the best-matched signal.

Step 4 Convergence judgment: This step controls the termination condition of the loop, to check if the estimation of the signal approaches stable, alternatively consecutive “update signal” stages give very similar estimates. If so, end the loop; otherwise, repeat from Step 2.

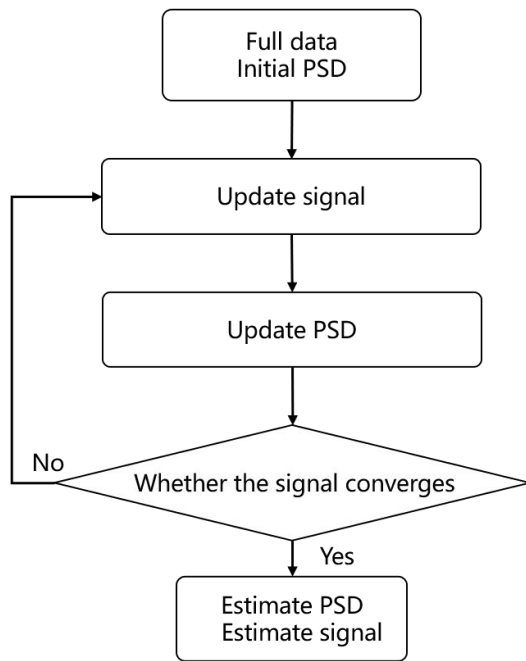


FIG. 1: Workflow of the iterative algorithm.

To search for the maximum of the posterior, we adopt the Particle Swarm Optimization (PSO) algorithm [72]. In this algorithm, particles representing solutions iterate through the solution space, refining their search directions based on individual and collective experiences. Ultimately, this process leads to the identification of potential optimal or nearly optimal solutions. The formula for updating particle positions is shown as follows. For the i -th particle, its position x_i and velocity v_i are updated in each iteration:

$$\begin{aligned} v_i(t+1) &= w \cdot v_i(t) + c_1 \cdot \text{rand}_1 \cdot (\text{pbest}_i - x_i) \\ &\quad + c_2 \cdot \text{rand}_2 \cdot (\text{gbest} - x_i), \\ x_i(t+1) &= x_i + v_i(t+1), \end{aligned} \quad (12)$$

where w represents the inertia weight, c_1 and c_2 are the learning factors, rand_1 and rand_2 are random numbers, pbest is the individual best position of particle, and gbest is the global best position of the entire group.

Inspired by the theoretical expression of the noise PSD, we perform a parametric estimation of the PSD, specifically targeting the position and acceleration noise parameters S_a and S_p . The estimation of these noise parameters is conducted using the PSO method, as detailed in Equation (9). Notice that the methodology is general and can be extended to a less model-dependent style.

The termination condition of the iterative algorithm relies on the convergence of the signals in two successive loops, and the fitting factor (FF) [73] is used to test the convergence of GW signal. FF is a measure used to evaluate how similar two waveforms are. The formula for calculating the FF is as follows:

$$FF = \frac{(h_1|h_2)}{\sqrt{(h_1|h_1)(h_2|h_2)}}. \quad (13)$$

Numerically, FF is limited in the range between -1 and 1, where 1 indicates a perfect match. The higher the degree of matching, the higher the degree of similarity between the assumed signal and the observed data. Termination occurs when the FF between the two signals reaches the specified threshold, the threshold for the FF is set as 0.99 in this paper.

C. Gapped data processing

In this part, we will introduce two methods for handling the gapped data: the window function and the inpainting technique. For comparison, we also present results on data that no treatment is applied. In this case, the likelihood is evaluated with frequency-domain waveforms, with the frequency components corresponding to the gap truncated.

1. Window function method

Similar to previous studies like [41], we use a Tukey-like window to handle the gapped data, as illustrated by Eq. 14.

$$w_{t_s}(t) \equiv \begin{cases} \frac{1}{2} \left(1 - \cos\left(\frac{2\pi t}{2t_w}\right)\right) & 0 \leq t < t_w \\ 1 & t_w \leq t < t_s - t_w \\ \frac{1}{2} \left(1 - \cos\left(2\pi \frac{t - t_s + 2t_w}{2t_w}\right)\right) & t_s - t_w \leq t < t_s \\ 0 & \text{otherwise,} \end{cases} \quad (14)$$

t_s represents the duration of each segment, and t_w is the smoothing time.

$$\mathbf{d}_{\text{win}} = \mathbf{d}_{\text{gap}} \cdot w_{t_s}(t). \quad (15)$$

The Tukey-like window function method can effectively prevent spectral leakage in the Fourier transform.

It achieves this by smoothing the data at the edges of the gaps. However, this can also result in the loss of valid data points around the gaps, resulting in a compromise in SNR. The data after using the window function method can be expressed as $\mathbf{d}_{\text{win}} = [d_1 \cdot w_{t_s}, \dots, d_{t_{\text{gap}}^i} \cdot w_{t_s}, 0, \dots, 0, d_{t_{\text{gap}}^f} \cdot w_{t_s}, \dots, d_N \cdot w_{t_s}]$, the covariance matrix Σ_{win} of \mathbf{d}_{win} fails to satisfy the circulant property. In principle, since Whittle's approximation fails, one should carry out calculations in the time domain. However, for convenience, we still adopt Whittle's approximation and evaluate likelihood in the frequency domain.

2. Gate-and-inpainting

The gate-and-inpainting technique, initially proposed by Zackay et al. [46], has been shown to effectively preserve inner product values when applied to open LIGO data [46]. This method masks the part of the covariance matrix associated with the problematic data, rendering it ineffective for matched filtering computations [48]. Isi and Farr [49] also applied the inpainting method to compute the inverse of the truncated covariance matrix. Kwok et al. [50] employed the inpainting filter to address false violations of General Relativity (GR) caused by short-duration, broadband glitches. Furthermore, Huber and Davis [47] also applied the inpainting technique to effectively mitigate the glitch problem by gating the glitch data and interpolating, reweighting, and normalizing the SNR of the gated glitch data segments. Similarly, drawing conclusions related to the quasi-normal modes requires removing portions of the dataset where the ringdown prescription is invalid, thus Capano et al. [51] applied the inpainting technique to ensure conclusions are not affected by gated inspiral-merger data. This method interpolates the data so that the likelihood after interpolation is equivalent to those before interpolation, without adding any additional information to the data.

In this work, we adopt the PyCBC realization of the inpainting to address the data gap issue Capano et al. [51]. In seeking to preserve the likelihood, the operation of data imputation from the inpainting technique helps suppress spectral leakage in the Fourier transform.

For instance, a data gap occurring during the time $t \in [t_{\text{gap}}^i, t_{\text{gap}}^f]$ in the event, the truncated noise can be represented as $\mathbf{n}_{\text{tr}} = [n_1, \dots, n_{t_{\text{gap}}^i}, n_{t_{\text{gap}}^f}, \dots, n_N]$. Subsequently, the log-likelihood defined in the time domain by Eq. (3) can be expressed with:

$$\mathbf{n}_{\text{tr}}^T \Sigma_{\text{tr}}^{-1} \mathbf{n}_{\text{tr}} = \mathbf{n}'^T \Sigma^{-1} \mathbf{n}', \quad (16)$$

\mathbf{n}' is the noise after inpainting, Σ and Σ_{tr} represent the covariance matrix of the full data and the truncated data.

To keep the value of likelihood unchanged after inpainting, it is required that

$$\begin{aligned} \Sigma^{-1} \mathbf{n}'[t] &= 0, t \in [t_{\text{gap}}^i, t_{\text{gap}}^f], \\ \Sigma^{-1} (\mathbf{d}' - \mathbf{h}') [t] &= 0, t \in [t_{\text{gap}}^i, t_{\text{gap}}^f], \end{aligned} \quad (17)$$

here \mathbf{d}' and \mathbf{h}' is the data and signal template after inpainting,

$$\begin{aligned}\mathbf{d}' &= \mathbf{d}_g \oplus \mathbf{d}_x, \\ \mathbf{h}' &= \mathbf{h}_g \oplus \mathbf{h}_x,\end{aligned}\quad (18)$$

where \mathbf{d}_g and \mathbf{h}_g are $1 \times N$ vectors, and \mathbf{d}_x and \mathbf{h}_x represent the data that fills in the gap with $1 \times M$ vectors. The symbols \oplus indicate the concatenation of the vector. According to Eq. (17), \mathbf{d}_x and \mathbf{h}_x can be solved by:

$$\begin{aligned}\overline{\Sigma^{-1}\mathbf{d}_x} &= -\overline{\Sigma^{-1}\mathbf{d}_g}, \\ \overline{\Sigma^{-1}\mathbf{h}_x} &= -\overline{\Sigma^{-1}\mathbf{h}_g}.\end{aligned}\quad (19)$$

The overbar indicates the $[t_{\text{gap}}^i, t_{\text{gap}}^f]$ rows (and columns) of the given vector (matrix). The advantage of using inpainting is that it involves solving for a $M \times M$ matrix rather than a $(N-M) \times (N-M)$ matrix. Since the number of gapped data M is much smaller than the total number N , this greatly reduces the computational burden. We used the PyCBC software to address inpainting data [51]. When solving for the inverse of the covariance matrix, the Levinson recursion was used to tackle the linear equation system. As a result, the computational complexity of the inpainting technique is reduced to $O(M^2)$ instead of $O(M^3)$.

IV. ESTIMATION RESULTS

In this section, we thoroughly investigate the results in scenarios where the gaps occur during different stages of the MBHB merger. We also present the results obtained by no treatment, the window method, and the inpainting method, respectively.

As revealed in previous studies, the result of the analysis is very sensitive to the position of the gap, since the accumulation of SNR becomes much quicker as the MBHB approaches the merger. A gap near the merger represents a much larger SNR loss compared with a gap far away from the merger. Therefore, we decided to study two scenarios as illustrated in Fig. 2. In the first case, the gap happens far away from the merger (the upper panel), and in the other case, the gap occurs adjacent to the merger, with the ending time coinciding with the merger time (the lower panel). The parameters of the signal are shown in Table I. The SNR of the full signal is 777.98.

A. PSD estimate from gapped data

In this part, we tested the iterative algorithm for estimating the noise PSD from gapped data. We injected the signal from Fig. 2 to noise and added corresponding gaps. When the gap happens far from the merger, the SNR is 777.96, almost identical to the full SNR. For the case where the gap happens close to the merger, the

TABLE I: The parameters of injected signal

Parameters	True
M_c/M_\odot	3×10^6
η	0.15
D_L/Gpc	10
ϕ_c/rad	$\pi/2$
λ/rad	π
β/rad	$\pi/3$
ψ/rad	$\pi/4$
ι/rad	$\pi/8$
t_c/s	207,360

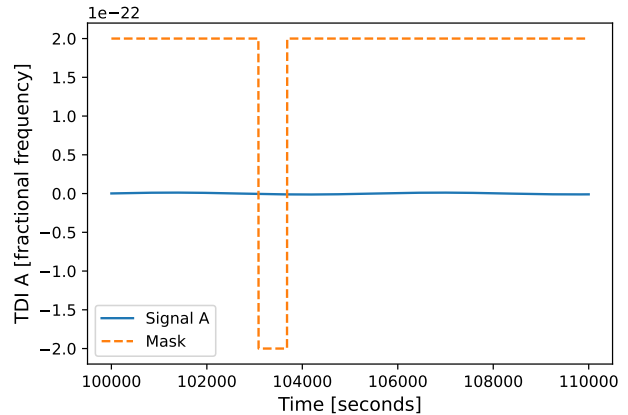
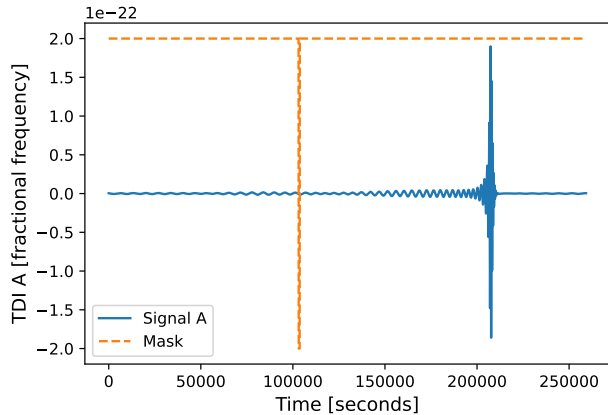
SNR becomes 487.87, much smaller than the full SNR. For either case, three methods, namely no treatment, window function method, and inpainting method are applied. As indicated in the flowchart (Fig. 1), an initial PSD is needed as a starting point, and we start with an extremely biased guess of the PSD, $1/S_n(f)$.

For either case, when no treatment is applied to the gap, the PSD estimation is biased, especially for the S_a , as the impact is most significant in the low frequency. On the other hand, utilizing the window function method and the inpainting method yields very similar values for both S_a and S_p to the injected value, the bias is smaller than 10%, often to the few percent level. We conclude also that the algorithm is very robust against the choice of the initial PSD.

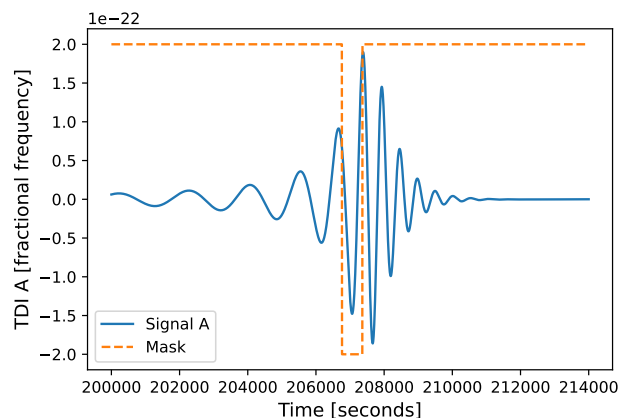
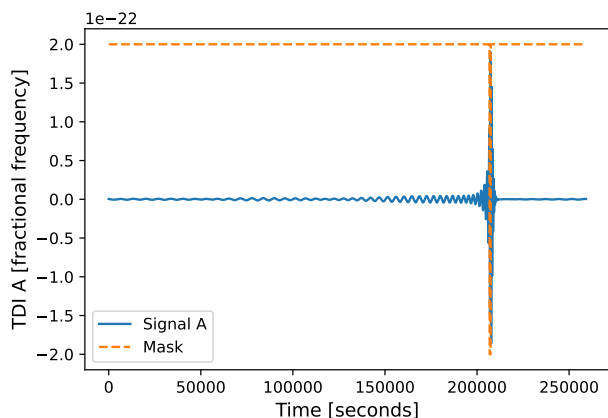
B. Results of gapped data estimation

Once we obtain an estimation of the noise PSD, we continue to perform parameter estimation of the MBHBs. Here we present the results for gapped data obtained with no treatment, the window method, and the inpainting method, separately. In this work, to make a fair comparison with previous studies like [41, 47], we only focus on the sky localization parameters.

For this purpose, we first show the posterior distribution for the source sky localization in Fig. 3. The upper panels are the results when the gap occurs far away from the merger, while the lower panels show results for the gap occurring at the merger. The left, middle, and right panels correspond to no treatment, the window function method, and the inpainting method, respectively. In all subplots, the color bar illustrates the difference of log-likelihood to the maximum, 1σ , 2σ , and 3σ credible regions were shown in contours. We can observe that in the results with no treatment, when the gap occurs far away from the merger, the injected parameter (indicated by the yellow star) is within the center of the credible regions even if the PSD estimation is incorrect. However, in scenarios with a gap occurring at the merger, even if the PSD estimation is close to the injected PSD, the injected parameters are far beyond the 3σ credible regions. This is because the gaps occurring at the merger loca-



(a) A gap occurring distant from the merger.



(b) A gap occurring adjacent to the merger.

FIG. 2: The images illustrate the relationship between the gap and the signal. The upper (lower) panels contain a gap located distant from (adjacent to) the merger. The right panels show the zoom-in figures around the gap. The blue solid lines are time domain waveforms, while the orange dashed lines indicate the window described with Eq. 11.

tion lead to more severe spectral leakage of the signal, resulting in a mismatch with the ideal frequency domain template. Both the window function and the inpainting methods give consistent estimates, with the injected parameter constrained within the center of the credible regions. When the gap occurs far away from the merger, both the window function method and the inpainting method can effectively recover the injected parameter. The two methods result in almost identical sizes and locations for the credible regions. On the other hand, in scenarios with the gap occurring at the merger, we observe much wider credible regions for the window function method than the inpainting method. This can be explained by the fact that the SNR of the MBHB accumulates much faster around the merger. The window function methods inevitably taper some part of the data, which leads to loss of information when that data contains a significant amount of SNR, and thus the widening of the credible regions. The figure is obtained by setting

the tapering length $t_w = 1000$ s. Finetuning the value of t_w may yield quantitatively different results, but the qualitative conclusions remain unchanged.

Next, we quantitatively examine the parameter estimation bias introduced by the methods. The difference between the injected parameter (red star) and the maximum (yellow star) in Fig. 3 does not overlap, and this bias can be explained by the intrinsic random fluctuation caused by the noise. However, treating the gap *per se* can potentially bring in bias. To separate this effect from the randomness raised by noise, we repeat the analysis on noise-free data and show results in Fig. 4. The maximum posterior of noise-free data for both the window function and inpainting methods are located at the same position as the true values, which indicates that the errors in both methods primarily arise from noise.

Finally, we aim to present a more realistic and useful result, to perform parameter estimation on an 11-dimensional space. For the first time, we obtain full di-

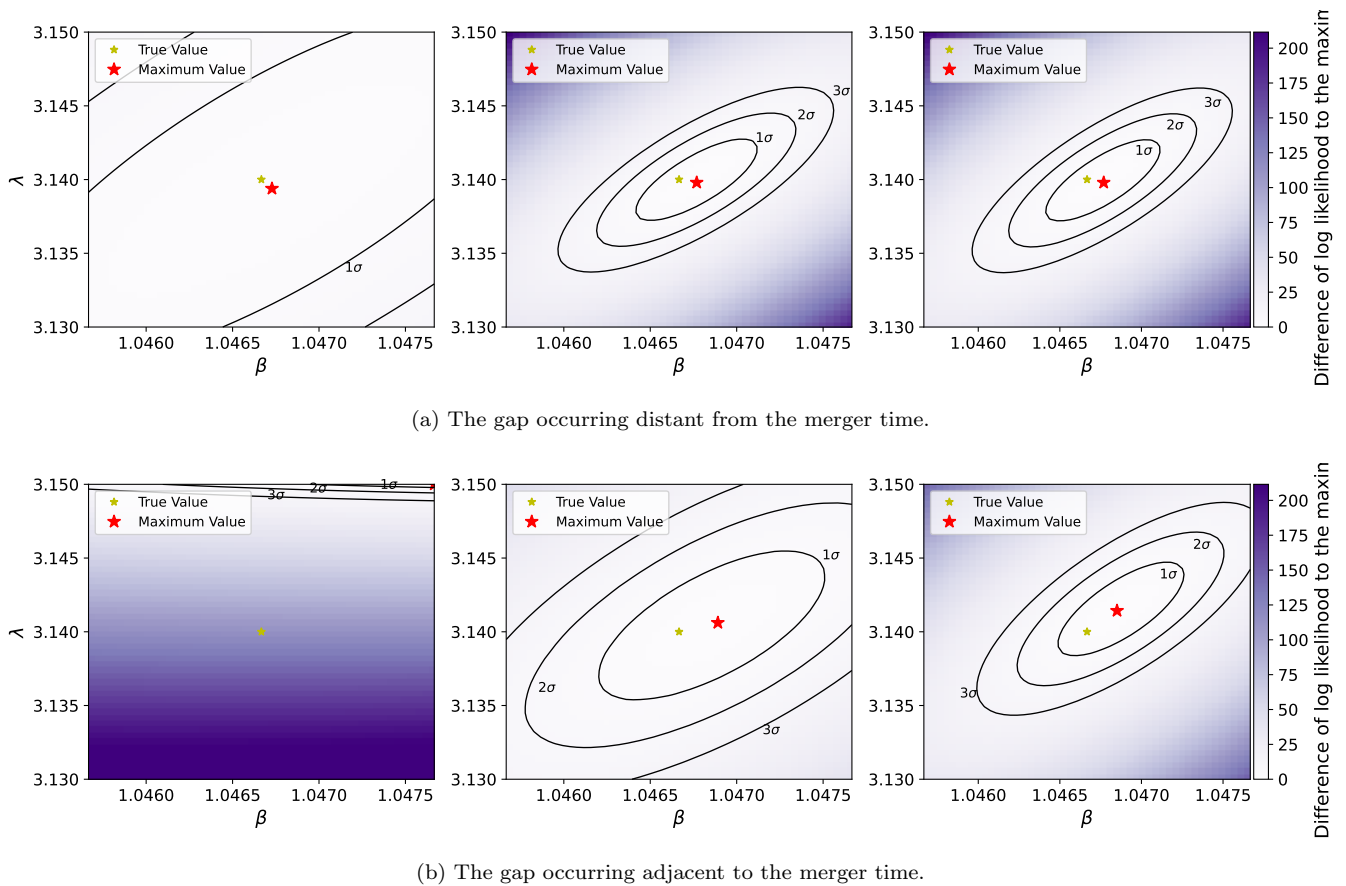


FIG. 3: The posterior distribution for the source sky localization. The left, middle, and right panels correspond to no treatment, the window function method, and the inpainting method, respectively. The red star indicates the positions of maximum posterior, the yellow star represents injected values, and the black lines denote 1σ , 2σ , and 3σ error ranges, respectively.

mensional parameter estimation results upon a gapped space-borne GW detector data, with noise included. We show the results in Fig. 5. The data set is identical to that of Fig. 3.b, with the gap happening during the merger. We adopt the `emcee` implementation of the affine-invariant Markov Chain Monte Carlo (MCMC) sampling algorithm [74] to stochastically sample the posterior distribution. The gap is filled by the inpainted data constructed by the estimated noise PSD as well as the waveform corresponding to the sampled parameter set. This means that for every likelihood evaluation, the inpainting method is executed. Thanks to the high efficiency of our inpainting implementation, 5×10^6 likelihood evaluations were performed within 40 hours on a 50 core cluster. In the figure, corner plots were shown for the marginalized 2-dimensional posterior distributions, the inner and outer contour lines represent 50% and 90% credible regions, respectively. On the top, the one-dimensional marginalized distributions were also shown. Blue lines which indicate the injected physical parameters are also drawn. We can observe that in all 1D plots, the injected values are correctly recovered within the 90% credible region. For the 2D plots, all injected val-

ues are recovered within the 90% credible region, while about half are within the 50% credible regions. We can compare with Fig. 3, and not surprisingly, the 2D posterior marginalized over all other dimensions is wider than the conditional 2D distribution. When comparing with previous studies on gap-free data, for example, Gao et al. [6], we can find that most of the 2D distributions are quite consistent, with most parameter precision agreeing within a factor of 3. There are three parameters that can differ by 1-2 orders of magnitudes: merger time t_c , polarization angle ψ , and inclination angle ι . The difference in polarization angle can be explained by the fact that our observation time (3 days) is significantly shorter than [6] (3 months). The weak constraining of the polarization angle leads to a poorly constrained inclination angle as well as the luminosity distance, as the degeneracy can not be broken. For our case, the merger time can be constrained to the level of ~ 100 s, while in Gao et al. [6] the precision is a factor of ten smaller. This is caused by the fact that we studied data corrupted by the gap, which exactly happens during the merger, so the core information of the merger time is missing.

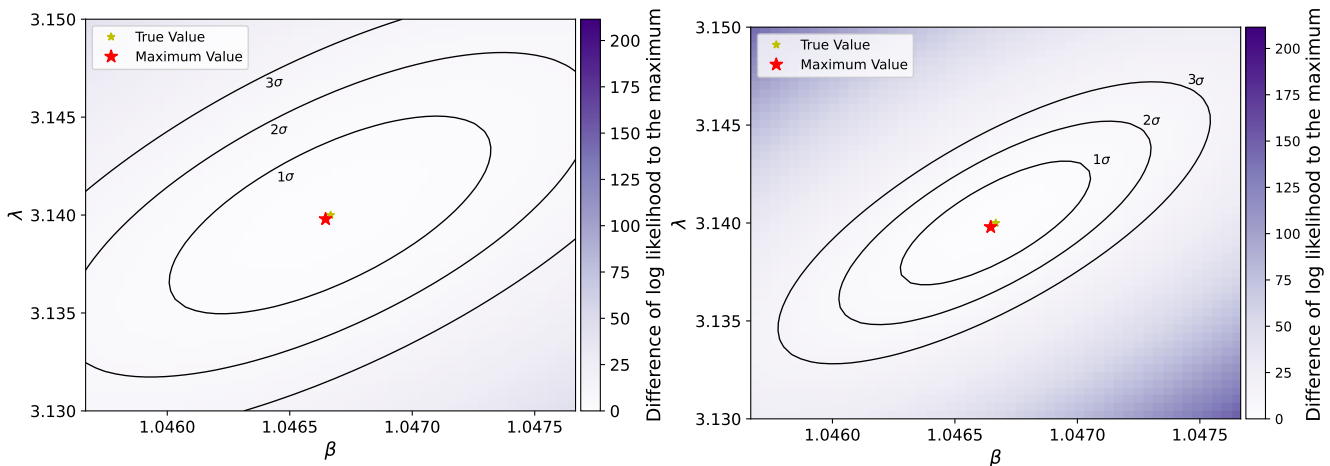


FIG. 4: Sky localization of the noise-free data with the window function method (left) and the inpainting method (right). Markers are defined in the same way as in Fig. 3

V. CONCLUSION

In this manuscript, we analyze the impact of data gaps on the parameter estimation of MBHBs for space-borne GW detectors, and experimented with two methods to deal with the gap. Under the iterative analysis framework for both the noise PSD and the signal, two methods, namely the window function method and the inpainting method, are implemented to deal with the gap. For the PSD estimation, the untreated data resulted in PSD estimation deviation, whereas employing the window function and inpainting methods produced PSD estimations consistent with the injected values.

With the PSD fixed, we perform parameter estimation for the MBHB signals, and all methods can appropriately estimate the injected parameters when the gaps occur far from the merger. However, when the gaps occur close to the merger, the untreated data leads to obvious deviations, while the window function and inpainting methods can both produce correct estimates where the 1σ credible regions contain the injected parameters.

In the case shown above, the spectral leakage of gaps in untreated data may lead to varying degrees of bias in the noise PSD estimation. When the gap occurs far away from the merger, with a relatively small loss in SNR, the likelihood estimation will still be close to the true value, even if the PSD is wrongly estimated. As the gap occurs at the merger, with a substantial loss in SNR, leads to more severe spectral leakage of the signal. In this case, even if the true PSD is adopted, the estimated signal is still biased. In contrast, both the window function and inpainting methods produce correctly estimated results. However, the tapering of the window function method contributes to SNR loss and consequently expands the credible range. The exact results are subject to the choice of smooth time t_w .

With this study, we find that the window function

method, which is easy to implement, can obtain an unbiased estimation of the parameters. It works especially well when the gap occurs far from the merger. This result differs from earlier studies but confirms observations from Dey et al. [21], while we took a step further in that realistic noise was included throughout the study. However, for gaps closer to the merger, the loss of some data points may result in an enlarged range of errors. Notably, the results of the above-mentioned windowed gapped data are based on several assumptions. In practice data processing, when employing the window function, the covariance matrix of windowed gapped data does not retain the Toeplitz property. Therefore, similar to gapped data, Whittle's approximation fails.

By employing an inpainting technique, the covariance matrix corresponding to the gaps is masked. The masked covariance matrix represents the true covariance matrix after data loss, thus preserving information on matching filter and likelihood. The computational cost of the likelihood is $O(N \log N)$, and the computational cost of inpainting is $O(M^2)$, where M is the number of missing data points.

The current limitation is that the noise model relies on a strong prior assumption, which has shortcomings in predicting or estimating the noise PSD. The estimation of noise PSD is based on maximum likelihood point estimation. Ideally, conclusions should be drawn after marginalizing over the PSD parameters, instead of based on a fixed estimate [41, 69]. Unfortunately, the implementation of such a target will require significantly larger computation resources, and we leave the development towards this target to future works.

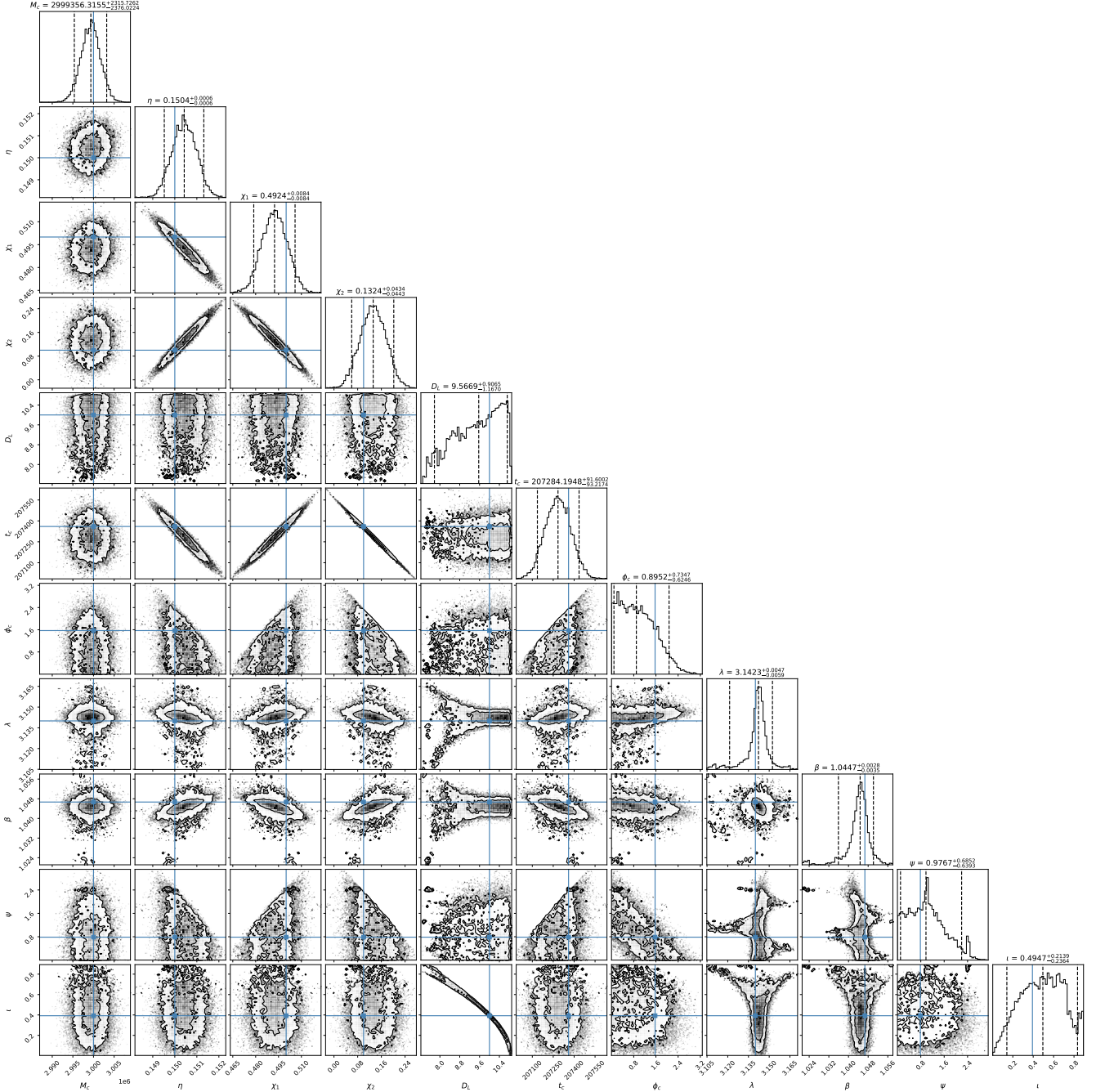


FIG. 5: The 11-dimensional parameter estimation results using the inpainting method for the case when the gaps occur at the merger. The blue line represents true values.

ACKNOWLEDGMENTS

The authors thank Yi-fan Wang and Jiandong Zhang for fruitful discussions at various stages of this work. Their expertise and valuable suggestions have provided crucial insights for this study. We also extend our gratitude to Liang Dai for equally invaluable discussions.

This work has been supported by the Guangdong Major Project of Basic and Applied Basic Research (Grant No. 2019B030302001), the Natural Science Foundation of China (Grant No. 12173104, No. 12261131504), and the Natural Science Foundation of Guangdong Province of China (Grant No. 2022A1515011862).

- [1] J. Luo et al., *Class. Quantum Grav.* **33**, 035010 (2016).
- [2] P. Amaro-Seoane, H. Audley, S. Babak, J. Baker, E. Barausse, P. Bender, E. Berti, P. Binetruy, M. Born, D. Bortoluzzi, et al., arXiv preprint arXiv:1702.00786 (2017).
- [3] H.-T. Wang, Z. Jiang, A. Sesana, E. Barausse, S.-J. Huang, Y.-F. Wang, W.-F. Feng, Y. Wang, Y.-M. Hu, J. Mei, et al., *Phys. Rev. D* **100**, 043003 (2019), URL <https://link.aps.org/doi/10.1103/PhysRevD.100.043003>.
- [4] W.-F. Feng, H.-T. Wang, X.-C. Hu, Y.-M. Hu, and Y. Wang, *Phys. Rev. D* **99**, 123002 (2019), URL <https://link.aps.org/doi/10.1103/PhysRevD.99.123002>.
- [5] H.-Y. Chen, X.-Y. Lyu, E.-K. Li, and Y.-M. Hu, arXiv preprint arXiv:2309.06910 (2023).
- [6] J. Gao, Y.-M. Hu, E.-K. Li, J.-d. Zhang, and J. Mei (2024), 2401.12813.
- [7] S.-J. Huang, Y.-M. Hu, V. Korol, P.-C. Li, Z.-C. Liang, Y. Lu, H.-T. Wang, S. Yu, and J. Mei, *Phys. Rev. D* **102**, 063021 (2020), URL <https://link.aps.org/doi/10.1103/PhysRevD.102.063021>.
- [8] Y. Lu, E.-K. Li, Y.-M. Hu, J.-d. Zhang, and J. Mei, *Research in Astronomy and Astrophysics* (2022).
- [9] S. Liu, Y.-M. Hu, J.-d. Zhang, and J. Mei, *Phys. Rev. D* **101**, 103027 (2020), URL <https://link.aps.org/doi/10.1103/PhysRevD.101.103027>.
- [10] X. Lyu, E.-K. Li, and Y.-M. Hu, arXiv preprint arXiv:2307.12244 (2023).
- [11] H.-M. Fan, Y.-M. Hu, E. Barausse, A. Sesana, J.-d. Zhang, X. Zhang, T.-G. Zi, and J. Mei, *Phys. Rev. D* **102**, 063016 (2020), URL <https://link.aps.org/doi/10.1103/PhysRevD.102.063016>.
- [12] Z.-C. Liang, Y.-M. Hu, Y. Jiang, J. Cheng, J.-d. Zhang, J. Mei, et al., *Phys. Rev. D* **105**, 022001 (2022).
- [13] J. Cheng, E.-K. Li, Y.-M. Hu, Z.-C. Liang, J.-d. Zhang, J. Mei, et al., *Phys. Rev. D* **106**, 124027 (2022).
- [14] R. Antonucci, *Annual review of astronomy and astrophysics* **31**, 473 (1993).
- [15] J. Kormendy and D. Richstone, *Annual review of astronomy and Astrophysics* **33**, 581 (1995).
- [16] F. Pacucci, B. Nguyen, S. Carniani, R. Maiolino, and X. Fan, *Astrophys. J. Lett.* **957**, L3 (2023), 2308.12331.
- [17] Y.-M. Hu, J. Mei, and J. Luo, *Natl. Sci. Rev.* **4**, 683 (2017).
- [18] C. Shi, J. Bao, H.-T. Wang, J.-d. Zhang, Y.-M. Hu, A. Sesana, E. Barausse, J. Mei, and J. Luo, *Phys. Rev. D* **100**, 044036 (2019), URL <https://link.aps.org/doi/10.1103/PhysRevD.100.044036>.
- [19] C. Shi, M. Ji, J.-d. Zhang, and J. Mei, *Phys. Rev. D* **108**, 024030 (2023), 2210.13006.
- [20] L.-G. Zhu, Y.-M. Hu, H.-T. Wang, J.-d. Zhang, X.-D. Li, M. Hendry, and J. Mei, *Physical Review Research* **4**, 013247 (2022).
- [21] K. Dey, N. Karnesis, A. Toubiana, E. Barausse, N. Korsakova, Q. Baghi, and S. Basak, *Phys. Rev. D* **104**, 044035 (2021).
- [22] D. Sigg, for the LIGO Scientific Collaboration, et al., *Classical and Quantum Gravity* **25**, 114041 (2008).
- [23] Q. Baghi, N. Korsakova, J. Slutsky, E. Castelli, N. Karnesis, and J.-B. Bayle, *Phys. Rev. D* **105**, 042002 (2022), 2112.07490.
- [24] M. C. Edwards, P. Maturana-Russel, R. Meyer, J. Gair, N. Korsakova, and N. Christensen, *Physical Review D* **102**, 084062 (2020).
- [25] Y. Jafry, T. Sumner, and S. Buchman, *Classical and Quantum Gravity* **13**, A97 (1996).
- [26] C. Speake, *Classical and Quantum Gravity* **13**, A291 (1996).
- [27] N. Robertson, J. Blackwood, S. Buchman, R. Byer, J. Camp, D. Gill, J. Hanson, S. Williams, and P. Zhou, *Classical and Quantum Gravity* **23**, 2665 (2006).
- [28] H. Yin, Y.-Z. Bai, M. Hu, L. Liu, J. Luo, D.-Y. Tan, H.-C. Yeh, and Z.-B. Zhou, *Physical Review D* **90**, 122001 (2014).
- [29] Z. Lihua, L. Ming, G. Yongxin, H. Yuexin, W. Fengbin, and Z. Tao, *ACTA SCIENTIARUM NATURALIUM UNIVERSITATIS SUNYATSENI* **60**, 129 (2021).
- [30] Q. Liu, j.-h. xu, L. Zhu, Q. Wang, Y. Zhang, S.-Q. Yang, and J. Luo, *Classical and Quantum Gravity* (2023).
- [31] S. Biscans, J. Warner, R. Mittleman, C. Buchanan, M. Coughlin, M. Evans, H. Gabbard, J. Harms, B. Lantz, N. Mukund, et al., *Classical and Quantum Gravity* **35**, 055004 (2018).
- [32] A. Schleicher, T. Ziegler, R. Schubert, N. Brandt, P. Bergner, U. Johann, W. Fichter, and J. Grzysimisch, *CEAS Space Journal* **10**, 471 (2018).
- [33] J. I. Thorpe, J. Slutsky, J. G. Baker, T. B. Littenberg, S. Hourihane, N. Pagane, P. Pokorny, D. Janches, M. Armano, H. Audley, et al., *The Astrophysical Journal* **883**, 53 (2019).
- [34] S. Hourihane, J. I. Thorpe, J. Slutsky, T. Littenberg, and J. Baker, in *American Astronomical Society Meeting Abstracts# 233* (2019), vol. 233, pp. 143–01.
- [35] S. Hourihane, T. Littenberg, J. G. Baker, N. Pagane, J. P. Slutsky, and J. I. Thorpe, in *AGU Fall Meeting Abstracts* (2017), vol. 2017, pp. P23B–2719.
- [36] M. Cabero, A. Lundgren, A. H. Nitz, T. Dent, D. Barker, E. Goetz, J. S. Kissel, L. K. Nuttall, P. Schale, R. Schofield, et al., *Classical and Quantum Gravity* **36**, 155010 (2019).
- [37] J. Glanzer, S. Banagiri, S. Coughlin, S. Soni, M. Zevin, C. P. L. Berry, O. Patane, S. Bahaadini, N. Rohani, K. Crowston, et al., *Classical and Quantum Gravity* **40**, 065004 (2023).
- [38] M. Armano, H. Audley, J. Baird, P. Binetruy, M. Born, D. Bortoluzzi, E. Castelli, A. Cavalleri, A. Cesarini, A. M. Cruise, et al., *Phys. Rev. Lett.* **120**, 061101 (2018), URL <https://link.aps.org/doi/10.1103/PhysRevLett.120.061101>.
- [39] T. Robson and N. J. Cornish, *Physical Review D* **99**, 024019 (2019).
- [40] Q. Baghi, N. Korsakova, J. Slutsky, E. Castelli, N. Karnesis, and J.-B. Bayle, *Physical Review D* **105**, 042002 (2022).
- [41] Q. Baghi, J. I. Thorpe, J. Slutsky, J. Baker, T. Dal Canton, N. Korsakova, and N. Karnesis, *Physical Review D* **100**, 022003 (2019).
- [42] J. Carré and E. Porter, arXiv preprint arXiv: 1010.1641, 2010 (2012).
- [43] D. Davis and M. Walker, *Galaxies* **10**, 12 (2022).
- [44] M. A. Tanner and W. H. Wong, *Journal of the American statistical Association* **82**, 528 (1987).
- [45] A. Bllelly, J. Bobin, and H. Moutarde, *Monthly Notices*

- of the Royal Astronomical Society **509**, 5902 (2022).
- [46] B. Zackay, T. Venumadhav, J. Roulet, L. Dai, and M. Zaldarriaga, *Phys. Rev. D* **104**, 063034 (2021).
- [47] M. C. Huber and D. Davis, arXiv e-prints pp. arXiv-2208 (2022).
- [48] T. Venumadhav, B. Zackay, J. Roulet, L. Dai, and M. Zaldarriaga, *Physical Review D* **100**, 023011 (2019).
- [49] M. Isi and W. M. Farr, arXiv preprint arXiv:2107.05609 (2021).
- [50] J. Y. Kwok, R. K. Lo, A. J. Weinstein, and T. G. Li, *rem* **42**, 1 (2021).
- [51] C. D. Capano, M. Cabero, J. Westerweck, J. Abedi, S. Kastha, A. H. Nitz, A. B. Nielsen, and B. Krishnan, arXiv preprint arXiv:2105.05238 (2021).
- [52] C. Pankow, K. Chatziioannou, E. A. Chase, T. B. Littenberg, M. Evans, J. McIver, N. J. Cornish, C.-J. Haster, J. Kanner, V. Raymond, et al., *Physical Review D* **98**, 084016 (2018).
- [53] R. M. Gray et al., *Foundations and Trends® in Communications and Information Theory* **2**, 155 (2006).
- [54] C. Hurvich, *Lecture Notes*, New York University Stern School of Business (2002).
- [55] A. Blelly, Ph.D. thesis, Université Paris-Saclay (2022).
- [56] S. Husa, S. Khan, M. Hannam, M. Pürrer, F. Ohme, X. J. Forteza, and A. Bohé, *Phys. Rev. D* **93**, 044006 (2016).
- [57] S. Khan, S. Husa, M. Hannam, F. Ohme, M. Pürrer, X. J. Forteza, and A. Bohé, *Phys. Rev. D* **93**, 044007 (2016).
- [58] M. R. Adams and N. J. Cornish, *Phys. Rev. D* **82**, 022002 (2010).
- [59] M. Vallisneri, *Phys. Rev. D* **71**, 022001 (2005), publisher: American Physical Society.
- [60] E.-K. Li, H. Wang, H.-Y. Chen, H. Fan, Y.-N. Li, Z.-Y. Li, Z.-C. Liang, X.-Y. Lyu, T.-X. Wang, Z. Wu, et al., arXiv preprint arXiv:2309.15020 (2023).
- [61] N. Christensen and R. Meyer, *Reviews of Modern Physics* **94**, 025001 (2022).
- [62] N. J. Cornish, T. B. Littenberg, B. Bécsy, K. Chatziioannou, J. A. Clark, S. Ghonge, and M. Millhouse, *Phys. Rev. D* **103**, 044006 (2021).
- [63] T. B. Littenberg and N. J. Cornish, *Phys. Rev. D* **91**, 084034 (2015).
- [64] Q. Baghi, N. Karnesis, J.-B. Bayle, M. Besançon, and H. Inchauspé, *Journal of Cosmology and Astroparticle Physics* **2023**, 066 (2023).
- [65] C. Roever, R. Meyer, and N. Christensen, *Classical and Quantum Gravity* **28**, 015010 (2010).
- [66] P. Welch, *IEEE Transactions on audio and electroacoustics* **15**, 70 (1967).
- [67] J. Veitch, V. Raymond, B. Farr, W. Farr, P. Graff, S. Vitale, B. Aylott, K. Blackburn, N. Christensen, M. Coughlin, et al., *Physical Review D* **91**, 042003 (2015).
- [68] T. Gupta and N. Cornish, arXiv preprint arXiv:2312.11808 (2023).
- [69] C. Plunkett, S. Hourihane, and K. Chatziioannou, *Physical Review D* **106**, 104021 (2022).
- [70] S. Biscoveanu, C.-J. Haster, S. Vitale, and J. Davies, *Physical Review D* **102**, 023008 (2020).
- [71] C. Talbot and E. Thrane, *Physical Review Research* **2**, 043298 (2020).
- [72] D. Bandopadhyay and C. J. Moore, arXiv preprint arXiv:2305.18048 (2023).
- [73] A. Buonanno, Y. Chen, and M. Vallisneri, *Phys. Rev. D* **67**, 104025 (2003).
- [74] D. Foreman-Mackey, D. W. Hogg, D. Lang, and J. Goodman, *Publications of the Astronomical Society of the Pacific* **125**, 306 (2013).